Optimum parameters for humic acid removal and power production by Al–air fuel cell electrocoagulation in synthetic wastewater

Wei Wei
Anhui Jianzhu University
Haoyang Gong
Anhui Jianzhu University
Lin Sheng
Anhui Jianzhu University
Dong Zhou
Anhui Jianzhu University
Shuguang Zhu (1780536279@qq.com)
Anhui Jianzhu University https://orcid.org/0000-0002-7404-8205

Research Article

Keywords: Aluminum–air fuel cell electrocoagulation, humic acid, wastewater treatment, power generation,

Posted Date: June 22nd, 2021

DOI: https://doi.org/10.21203/rs.3.rs-578503/v1

Version of Record: A version of this preprint was published at Water Science and Technology on November 29th, 2021. See the published version at https://doi.org/10.2166/wst.2021.495.

Abstract

Although humic acid (HA) is a complex natural organic matter, it can potentially harm the environment and human health. In this study, aluminum–air fuel cell electrocoagulation (AAFCEC) was used to remove HAs from water while generating electricity. This device can generate electricity from the anodic oxidation of aluminum without an external power source as well produce an aluminum coagulant. Operating parameters, namely initial pH, electrolyte concentration, and HA concentration, were analyzed to determine the optimal power generation and removal efficiency. Al–Ferron complexation timed spectrophotometry was used to determine the Al speciation distribution in the solution. The power density of the cell reached 313.47 mW/cm^2 for the following conditions: 1 g/L NaCl concentration, 3 cm electrode distance, 20 Ω external resistor, and pH 9. And after about an hour electrolysis, the optimum removal rate of HA was above 99%. The results demonstrate that the AAFCEC is an efficient and eco-friendly water treatment process, and it could be further developed and disseminated in the rural areas and households.

1. Introduction

Humic acids (HAs) are complex natural organic matter formed from the remains of various plants and animals by anaerobic respiration of microorganisms in water, soil, and other environments(Afef et al.2019; Son et al.2019). HAs exist in large quantities in water, accounting for approximately 40–90% of the soluble organic pollutants in water (Hamed et al.2019). The main HA components are carbon, hydrogen, oxygen, nitrogen, and a small amount of phosphorus, sulfur, and other elements. HA has no fixed molecular structure. It is generally believed that the core structure of HA consists of aliphatic and aromatic parts, surrounded by various functional groups, such as hydroxyls, phenols, carboxyls, and ketones (Xie et al.2020; Liu et al.2020; Manuel et al.2020). These functional groups can adsorb organics and heavy metal ions in the water to form chelates that are difficult to remove (Zhang et al.2020; Zhou et al.2021). A large amount of HA can significantly affect the color, smell, and taste of water. In addition, HA in drinking water can form trihalomethanes, haloacetic acids, and other disinfection byproducts during the disinfection process, and these substances can potentially endanger human health (Aunnop et al.2018; Zhao et al.2020; Song et al.2019). Therefore, HAs should be removed from the water to reduce its potential harm to the environment and human body.

There are several techniques to remove HAs from water, including adsorption (Surendra et al.2020; Elham et al.2018), membrane filtration (Hwang et al. 2013), advanced oxidation (Yin et al.2020), ion exchange (Wang et al.2009), and coagulation (Xu et al.2016; Kanika et al.2019). However, these methods have some disadvantages, such as long processing time, high processing cost, difficult process control, and secondary pollution. Considering these problems, a more effective removal method is needed. According to previous research (Abdellatif et al.2020; Feride et al.2017), electrocoagulation (EC) is a technology that can effectively remove HA. EC is a simple and effective electrochemical process in which flocculants are produced by the electrolysis of metal anodes. As an eco-friendly water treatment technology, EC is widely used to remove various pollutants from water bodies, such as arsenic

(Emilijan et al.2018; E. Şık et al.2017), chromium (A. Martín-Domínguez et al.2018), cadmium (Subramanyan et al.2011), phosphate (Adelaide et al.2019), nitric acid salts (Ismahane et al.2019), dyes (Murat et al.2009), fluorides (João et al.2018), and chemical oxygen demand (M. Elazzouzi et al.2017). Compared with traditional chemical coagulation, EC can generate coagulants through the electrolysis of metal anodes without the addition of chemicals. EC has the advantages of simple equipment requirement, convenient operation, easy control, and short running time. However, the operation of EC requires a large amount of electric energy, which limits its development. Therefore, it is necessary to reduce the power consumption of EC, thereby facilitating the application of this technology.

To reduce the EC power consumption, this study combines the concepts of metal–air fuel cells and electrocoagulation to design an aluminum–air fuel cell electrocoagulation (AAFCEC) equipment. The device, which consists of an aluminum anode and an air cathode, can generate electricity from the anodic oxidation of aluminum without an external power source, and it can also produce an aluminum coagulant. As a new type of energy cell, the aluminum–air fuel cell has the advantages of high specific energy and specific power, less harm to the environment, simple cell structure, safety, and reliability (Wu et al.2020; Petros et al.2020). The aluminum plate is used as the electrode because aluminum has advantages such as abundant reserves, low price, and nontoxicity (Wu et al.2020). In addition, the aluminum salt produced in the reaction is an effective coagulant and can potentially be used to remove pollutants from water. Aluminum–air batteries can generate electricity because of the low oxidation potential of aluminum and the relatively high reduction potential of oxygen. There is a potential difference between the two electrodes, which causes the electrons to continuously flow from negative to positive, thereby forming a continuous current. The reaction formula is shown in (1)–(3)(P. Goel et al.2020).

Anode: $Al(s) + 3OH^-(aq) \rightarrow Al(OH)3(s) + 3e^-$ E_0=-2.35V (1)

Cathode: $O_2(g) + 2H_2O(l) + 4e^- \rightarrow 4OH^-(aq)$ E_0= +0.40V (2)

Overall reaction: $4Al(s) + 3O_2(g) + 6H_2O(l) \rightarrow 4Al(OH)_3(s)$ E_0= -2.75V (3)

The purpose of this study is to explore the feasibility and optimal conditions of an AAFCEC for the removal of HA from wastewater and to investigate the potential power generation of its cell. We investigated the influence of different parameters on electricity generation performance to determine the optimum conditions for power generation. We also determined the form of Al in the solution by using Al–Ferron complexation timed spectrophotometry. Subsequently, we investigated the removal efficiency of HA under different reaction conditions to determine the optimum removal conditions. Finally, we compared the results and proposed an appropriate set of parameters for an optimum balance between HA removal efficiency and power generation.

2. Experiment And Methods

2.1 Sample

The HA sample used in the experiments was artificially configured. HA was dissolved in deionized water in a beaker and continuously stirred with a magnetic agitator. The obtained solution was then filtered through a 0.45 μm filter membrane, and the obtained filtrate was the HA stock solution, which was refrigerated. In the experiments, sodium chloride solution was used as the electrolyte, and 0.1 M HCl and 0.1 M NaOH were used to adjust the pH of the solution to prevent other ions from being introduced and affecting the experimental results. All materials used in the experiments were of analytical grade.

2.2. Experimental setup and procedures

The experimental device was a rectangular parallelepiped with size of 180 mm× 30 mm × 180 mm, which was hollow inside in a cylinder format with diameter of 15 mm and height of 3 cm. The front and rear sides were composed of square organic glass plates that formed a closed container. The effective volume of the device was 800 mL. The aluminum plate anode (100 mm × 100 mm × 0.25 mm) was polished with sandpaper before the experiments and cleaned with absolute ethanol. The air electrode was composed of carbon black and activated carbon. Polytetrafluoroethylene was used as a binder. Platinum and copper were added as catalysts to the carbon powder of the catalytic layer. The carbon powder was laminated and fixed by a roller press on a nickel metal net.

In the experiment, a static aluminum–air fuel cell was constructed. Its power generation was explored by adjusting different parameters, such as NaCl concentration (0.5, 1, 2, and 3.5 g/L), initial pH (5, 6, 7, 8, and 9), electrode distance (3, 6, 9, and 12 cm), and external resistance (10, 20, and 50 Ω), which provided a technical basis for the subsequent experiments. Simultaneously, the total aluminum concentration and the aluminum form distribution were investigated under different conditions to determine the relationship between electricity production and aluminum production. The HA water sample was then placed in a beaker, and its Ph(5,6,7,8 and 9), NaCl concentration(0.5, 1, 2, and 3.5 g/L), and initial concentration(5mg/L, 10mg/L, 20mg/L and 40mg/L)were adjusted to determine the removal efficiency. Subsequently, 10 mL HA solution was directly sampled from the beaker using a syringe at reaction times of 15, 30, 45, 60, 120, and 180 min. The samples were filtered through a 0.45 μm filter membrane, and their respective HA content were measured. All the experiments were triplicate at least, and the average were been reported.

2.3. Analysis and calculation

The voltage of the resistor was collected by a data acquisition card connected to a computer. The data acquisition card collected voltage data every 0.5 s, and all voltage values were stored in the computer for subsequent processing.

Linear sweep voltammetry was used to measure the power density and polarization curves using an electrochemical workstation with an aluminum anode as the working electrode, an air cathode as the counter electrode, and a saturated calomel electrode as the reference electrode. The measurement range

was set from the open circuit voltage (−0.7 to −0.8 V) to 0 V, and the sweep gradient was set to 0.01 V. The current density (i) and power density (P) were calculated using the following equations:

$$i = U/(RA), \quad (4)$$

$$P = iU, \quad (5)$$

where U is the voltage (mV), R is the external resistance (Ω), and A is the surface area of the anode (cm^2). Therefore, considering the current density as the abscissa and the power density as the ordinate, the power density curve was obtained.

The aluminum form was determined by Al–Ferron complexation timed spectrophotometry. The aluminum form can be divided into three types: Ala, Alb, and Alc. Ala is a monomer form of aluminum, and it mainly includes Al^{3+} and $AlOH^{2+}$; Alb is a polymer form, mainly including Al_2OH_4, Al_6OH_{12}, and $Al_{13}OH_{32}$; Alc is the aluminum in the form of sol or gel, mainly including $Al(OH)_3$. UV_{254} was measured with an ultraviolet spectrophotometer at a 254 nm wavelength to represent the HA concetration.

3. Results And Discussion

3.1. Electrochemical analysis

3.1.1 Effect of electrolyte concentration

The voltage values according to time for different NaCl concentrations are shown in **Fig.1**. Evidently, as the concentration of NaCl increases, the voltage also increases. When the NaCl concentration was 0.5, 1, 2, and 3.5 g/L, the initial voltages were 145, 207, 257, and 306 mV, respectively. This may be attributed to the solution conductivity, which increased with increasing electrolyte concentration. Therefore, the electron transfer rate increased correspondingly. In the first 15 min of reaction, the voltage increased slightly, after which it gradually stabilized. The stable voltages were 167, 229, 306, and 342 mV.

As shown in **Fig.2(a)**, the maximum power density of the cell increased significantly as the electrolyte concentration increased. When the NaCl concentration was 0.5, 1, 2, and 3.5 g/L, the corresponding maximum power densities were 108.97, 169.36, 272.08, and 427.59 mW/cm^2. These results are consistent with the changes in the anode potential. **Fig.2(b)** shows the polarization curves for different NaCl concentrations. When the NaCl concentration increased, the trend of the polarization curve was relatively smooth. This implies that for the same current density, the power generation is better at higher electrolyte concentrations.

Usually, the aluminum electrode surface is covered with a corrosion-protective film composed of oxide or hydroxide. The existence of this protective film hinders the charge transfer between electrode and solution, increasing the ohmic resistance and anode electrode potential. Therefore, proper removal of this protective layer is conducive to the electrode reaction. According to previous studies (Kim et

al.2018; Kim et al.2017; Hubdar et al.2019), NaCl is one of the most effective electrolytes for such removal. The Cl^- in the solution reacts with the protective film to accelerate the dissolution rate of the aluminum anode, as shown in formulas (6)–(10) (Hubdar et al.2018). Therefore, NaCl reduces the ohmic resistance of the electrolyte and improves the electron transfer efficiency. Consequently, the cell obtains a higher power density. These conclusions are consistent with our experimental results.

$$Al_2O_3 + 6Cl^- + 6H^+ \rightarrow AlCl_3 + H_2O \quad (6)$$

$$Al(OH)_3 + Cl^- \rightarrow Al(OH)_2Cl + OH^- \quad (7)$$

$$Al(OH)_2Cl + Cl^- \rightarrow Al(OH)Cl_2 + OH^- \quad (8)$$

$$Al(OH)Cl_2 + Cl^- \rightarrow AlCl_3 + OH^- \quad (9)$$

$$AlCl_3 + Cl^- \rightarrow AlCl_4^- \quad (10)$$

3.1.2 Effect of initial pH

We explored the effects of initial pH on the power generation of the Al–air fuel cells. The changes in voltage according to time are shown in **Fig.3**. Weak acid or weak alkaline electrolytes were more conducive to electricity generation than that in the neutral electrolyte. In contrast, neutral electrolyte led to a relatively poor power generation performance. For an initial pH of 9, the voltage was the highest, and the corresponding stable voltage reached 247 mV. When the initial pH was 5, the stable voltage reached 244 mV. The cell showed the worst performance at pH 7. Overall, the voltage was not significantly different at different initial pH values.

Similar results were observed for the power density curve and polarization curve. As shown in **Fig.4(a)**, for initial pH of 9, the power density was the maximum, reaching 326.10 mW/cm^2. At pH 5, the second highest power density of 313.47 mW/cm^2 was obtained. For initial pH of 7, the power density was the smallest, at 267.807 mW/cm^2. The relative anode potentials at different initial pH values presented similar results. As shown in **Fig.4(b)**, the anode potential for weak acid and alkaline electrolytes increased slowly, which is consistent with the results described above.

In other words, the electricity generation performance of the aluminum–air fuel cell was better in weak acid and alkaline electrolytes. This may been attributed to the corrosion protection layer on the surface of the aluminum anode, which reacts with the hydrogen or hydroxide ions in the weak acid and alkaline electrolyte, thereby dissolving the protection layer. Consequently, the cells obtained superior power generation. However, in a neutral electrolyte, the protective layer of the aluminum sheet hardly reacted, and the electricity generation performance was relatively poor.

3.1.3 Effect of electrode distance and external resistance

To explore the effect of electrode distance on cell power generation, experiments were performed with electrode spacing of 3, 6, 9, and 12 cm. **Fig.5** shows that the voltage decreased significantly with the increase in electrode distance. For the electrode distance of 3 cm, the voltage reached its maximum, at approximately 300 mV. For electrode spacing of 12 cm, the stable voltage reached only 190 mV. This occurred because the internal resistance increased with the electrode distance, thereby increasing the energy consumption(Khalid et al.2017; Khalid et al.2017; Khalid et al.2019). We used voltammetry to roughly measure the cell internal resistance; the results are shown in **Fig.6**. The slope of the fitted volt–ampere characteristic curve was used to roughly estimate the internal resistance of the fuel cell. For electrode distances of 3, 6, 9, and 12 cm, the internal resistances were approximately 12, 18, 25, and 32 Ω, respectively. Therefore, electrode spacing significantly impacts the aluminum–air cell, and we set the electrode spacing to 3 cm in the subsequent experiments to obtain a better power generation.

We investigated the influence of external resistors on the power generation of the aluminum–air cell. The voltage and power according to time at different external resistances are shown in **Fig.7**. The highest voltages were obtained under external resistance of 50 Ω, reaching 420 mV; however, the output power was very low at that resistance. In contrast, lower voltages and higher powers were obtained at 10 Ω. Therefore, to provide a considerable output power and ensure a high stable voltage, the subsequent experiments used an external resistance of 20.

3.2 Aluminum speciation

Al species are crucial in the EC process as they determine the behavior and efficiency of Al-based coagulants (He et al.2016; Kong et al.2021). Formulas (1)–(3) show that the anode dissolves to generate Al^{3+} into the solution, and Al^{3+} is hydrolyzed to form various forms of compounds or polymers. The aluminum species is essential to determine whether the EC can remove HAs. This study investigates the optimum operating parameters according to the distribution of aluminum speciation in the solution.

Fig.8 shows the distribution of aluminum speciation according to time for different NaCl solution concentrations at pH 5. As the reaction progressed, the concentrations of Ala, Alb, and Alc gradually increased. The concentration of Alc increased quickly and reached the highest amount at the end. The contents of Ala and Alb were relatively low, and their growth was relatively slow, and it even presented a downward trend after some time. This can be explained by the fact that Ala and Alb in the solution are continuously converted into Alc as the reaction progresses. The final Al concentration indicates that all aluminum species in the solution increased with the NaCl concentration. When the NaCl concentration reached 3.5 g/L, the concentrations of Ala, Alb, and Alc reached 1.131, 8.145, and 16.147 mg/L, respectively.

To explore the effect of pH on the Al species, the initial solution pH was adjusted to 5, 6, 7, 8, and 9 using dilute hydrochloric acid and dilute sodium hydroxide. In the experiments, a 3.5 g/L NaCl solution was used as the electrolyte. **Fig.9** shows that the concentration of all Al species in the solution have increased. The total aluminum concentration was the highest at pH 9. As described in Section 3.1, the fuel cell

presented the best electricity production performance at this pH. In general, the total aluminum concentration did not significantly change according to pH.

We also observed that the concentration of Alc was higher when the electrolyte was weakly alkaline. At pH 9, the concentration of Alc reached 20.163 mg/L. The content of Ala and Alb in the weakly acidic electrolyte was relatively higher than that in the weakly alkaline electrolyte. This may be attributed to the hydrolysis reaction of Al^{3+}. According to previous studies (Hu et al.2012), the main hydrolysis products of Al^{3+} are different at different pH values. This may be explained by the presence of H^{+}, which inhibits the conversion of Ala to Alc in an acidic solution. Therefore, Al^{3+} and $AlOH_2^{+}$ were dominant in the solution. Moreover, as the pH value of the solution increases, the increase in OH^{-} promoted the formation of $Al(OH)_3$, and the concentration of Alc gradually increased.

3.3 HA removal

According to previous studies electrolyte (B.K. Zaied et al.2020; Hubdar et al. 2019), concentration is an important factor of EC. As shown in **Fig.10(a),** the HA removal efficiency significantly improved with increasing NaCl concentration. When the NaCl concentration was 3.5 and 2 g/L, the HA removal was over 90% in approximately 30 min of reaction. After approximately 40 min, the HA removal rate was approximately 95% for all samples, except for those with NaCl concentration of 0.5 g/L. Therefore, the use of a higher concentration of NaCl solution can significantly improve the removal efficiency of the AAFCEC.

This phenomenon can be explained by the higher ion concentration in the solution, which significantly increases the conductivity, thereby significantly improving the transfer rate of electrons on the electrode surface (N.P.Tanattı et al.2018) . Correspondingly, the dissolution rate of the anode also increases, as well the amount of aluminum flocculant. Cl^{-} has the potential to break down the protective layer at the surface of the metal anode electrodes to remarkably increase the current density (Kim et al.2015). In addition, as described in 3.2, the concentration of the NaCl solution also affects the speciation distribution of Al. As the concentration of the NaCl solution increases, the total aluminum concentration, especially the concentration of Alc, also significantly increases. According to previous studies (Sergi et al.2017), Al(OH)3 is the main coagulant in Alc , and it is essential for the electro-flocculation process. According to our experiments, when the NaCl concentration is greater than 1 g/L, most HAs can be removed, and a higher power generation can be obtained. Therefore, considering the economic benefits, the subsequent experiments were performed using 1 g/L NaCl solution.

The effect of initial HA concentration is shown in **Fig.10(b)**. We prepared HA samples of 5, 10, 20, and 40 mg/L to investigate the effect of different HA concentrations on the removal efficiency. After 3 h of reaction, the HA removal rate in the solution at different initial concentrations surpassed 96%. When the HA concentration was less than 20 mg/L, the removal rate was higher than 90% after 60 min. For this reaction time, the 40 mg/L HA sample presented a removal rate smaller than 50%. Therefore, 20 mg/L was the best initial HA concentration, and it was used in the subsequent experiments.

The pH can significantly affect the EC process, which can affect the Al hydrolysate and HA structure (Antonio et al.2020; Ali et al.2008). The effect of HA removal at different pH values is shown in **Fig.10(c)**. The initial pH value presented a certain effect on the HA removal. After the reaction proceeded for 120 min, the UV_{254} values all dropped to a lower level, which indicated that the HAs were removed. Although the HA removal efficiency in the acidic solution was slightly higher than that in the alkaline solution, the overall difference was not significant. A relatively higher removal efficiency of HA was observed at pH 5. This is also consistent with the results of previous studies (Antonio et al.2020). This phenomenon can be explained by the formation of a gel layer on the surface of the aluminum anode under high pH and high HA concentration. At pH 5, the presence of H^+ can inhibit the formation of the gel layer. In addition, as mentioned in Section 3.1, the aluminum–air fuel cell has a relatively good power generation at pH 5. Furthermore, the total aluminum concentration in the solution is relatively high at this pH. Therefore, pH 5 was considered the optimum pH value.

4 Conclusions

In this study, we determined the optimal AAFCEC parameters for power generation and HA removal.Based on economic aspects and HA removal, we adjusted the relevant parameters to 1 g/L NaCl concentration, pH 5, and initial HA concentration of 20 mg/L, at which the power density reached 313.47 mW/cm^2, and the HA removal rate was over 99%. Our results indicate that AAFCEC is a green and efficient water treatment process that can be used to remove HAs from water. And this device has a great advantage on wastewater treatment of rural areas or households because of its no need for external power supply.

Declarations

Ethics approval and consent to participate: Not applicable.

Consent to Publish: Not applicable.

Funding: This research was funded by University Natural Science Research Project of Anhui Province (CN) (NO.KJ2019A0756) ; Research Project Fund of Anhui Jianzhu University, Hefei, China (NO.2018QD08) and Natural Science Foundation of Anhui Province (CN) (NO. 1908085QE249); Key Research and Development Program of Anhui Province - General Key Project (201904a07020070).

Author Contributions: Conceptualization, Wei Wei; Formal analysis, Shuguang Zhu and Wei Wei; Funding acquisition, Wei Wei; Methodology, Haoyang Gong; Project administration, Haoyang Gong; Resources, Lin Sheng and Dong Zhou; Validation, Wei Wei; Writing – original draft, Haoyang Gong.

Conflicts of Interest: The authors declare that they have no known competing financial interests or personal relationships that could have appeared to influence the work reported in this paper.

Vailability of data and materials: All data generated or analysed during this study are included in this published article [and its supplementary information files]. And that the content of the article and the

experimental data are authentic.

References

Abdellatif El-G, Mohammad A, Ahmed K , Ignasi S, Ahmed AW, Corrosion behavior of pure titanium anodes in saline medium and their performance for humic acid removal by electrocoagulation. Chemosphere 246 (2020) 125674. https://doi.org/10.1016/j.chemosphere.2019.125674

Adelaide D, Carmel B. B, Electrocoagulation using stainless steel anodes: Simultaneous removal of phosphates, Orange II and zinc ions, Journal of Hazardous Materials 374 (2019) 152–158. https://doi.org/10.1016/j.jhazmat.2019.04.032

Afef B, Sana N, Amel C, Khaled B, Wided B, Elimame E,High-rate humic acid removal from cellulose and paper industry wastewaterby combining electrocoagulation process with adsorption onto granular activated carbon, Industrial Crops & Products 140 (2019) 111715. https://doi.org/10.1016/j.indcrop.2019.111715

Ali Savas K, Yalcın SY, Bülent K, Nuhi D, Effect of initial pH on the removal of humic substances from wastewater by electrocoagulation, Separation and Purification Technology 59 (2008) 175–182. https://doi.org/10.1016/j.seppur.2007.06.004

A. Martín-Domínguez, M.L. Rivera-Huerta , S. Pérez-Castrejón, S.E. Garrido-Hoyos, I.E. Villegas-Mendoza, S.L. Gelover-Santiago, P. Drogui b, G. Buelna, Chromium removal from drinking water by redox-assisted coagulation:Chemical versus electrocoagulation, Separation and Purification Technology 200 (2018) 266–272. https://doi.org/10.1016/j.seppur.2018.02.014

Antonio G. M, Brunno F. S, Artur S.C. R, Ronald R. H, Maurı´cio L. T, Treatment of oily wastewater from mining industry using electrocoagulation: Fundamentals and process optimization, journal of materials research and technology 9 (2020) 15164-15176. https://doi.org/10.1016/j.jmrt.2020.10.107

Aunnop W, Pharkphum R, Alongorn S, Adisak S, Synthesis of porous Pig bone char as adsorbent for removal of DBPs precursors from surface water, Water Science & Technology 486 (2018) 510589. https://doi.org/10.2166/wst.2018.486

B.K. Zaied, M. Rashid, M. Nasrullah, A.W. Zularisam, D. Pant, L. Singh, A comprehensive review on contaminants removal from pharmaceutical wastewater by electrocoagulation process, Science of the Total Environment 726 (2020) 138095. https://doi.org/10.1016/j.scitotenv.2020.138095

Elham D, Ali N, Optimization of humic acid removal by ad- sorption onto Bentonite and Montmorillonite nanoparticles, 259 (2018) 76-81. https://doi.org/10.1016/j.molliq.2018.03.014

Emilijan M, Srdjan R, Jasmina A, Kristiana Z, Aleksandra T, Božo D, Arsenic removal from groundwater by horizontal-flow continuous electrocoagulation (EC) as a standalone process, Journal of Environmental

Chemical Engineering 6 (2018) 512–519. https://doi.org/10.1016/j.jece.2017.12.042

E. Şık, E. Demirbas b, A.Y. Goren, M.S. Oncel, M. Kobya, Arsenite and arsenate removals from groundwater by electrocoagulation using iron ball anodes: Influence of operating parameters, Journal of Water Process Engineering 18(2017) 83–91. http://dx.doi.org/10.1016/j.jwpe.2017.06.004

Feride UK, Mehmet K, Erhan G, Removal of humic acid by fixed-bed electrocoagulation reactor: Studies on modelling, adsorption kinetics and HPSEC analyses, Journal of Electroanalytical Chemistry 804 (2017) 199–211. http://dx.doi.org/10.1016/j.jelechem.2017.10.009

Hamed S, Amir HM, Kamyar Y, Abbas A, Kiomars S, Mahmood A, Mirzaman Z, Effect of modification by five different acids on pumice stone as natural and low-cost adsorbent for removal of humic acid from aqueous solutions - Application of response surface methodology, Journal of Molecular Liquids 290 (2019)111181. https://doi.org/10.1016/j.molliq.2019.111181

He Z, Lan H, Gong W, Liu R, Gao Y, Liu H, Qu J, Coagulation behaviors of aluminum salts towards fluoride:Significance of aluminum speciation and transformation, Separation and Purification Technology 165 (2016) 137-144. http://dx.doi.org/10.1016/j.seppur.2016.01.017

Hubdar AM, Kim JH, An BM, Park JY, Effects of supporting electrolytes in treatment of arsenate-containing wastewater with power generation by aluminumair fuel cell electrocoagulation, Journal of Industrial and Engineering Chemistry 57 (2018) 254–262. http://dx.doi.org/10.1016/j.jiec.2017.08.031

Hubdar AM, Kim JH, Kim K, Park JY, Azmatullah K, Metal-air fuel cell electrocoagulation techniques for the treatment of arsenic in water, Journal of Cleaner Production 207 (2019) 67-84. https://doi.org/10.1016/j.jclepro.2018.09.232

Hubdar AM, Lee J, Park JY, Kim JC, Kim KH, Kim JH, An energy-efficient air-breathing cathode electrocoagulation approach for the treatment of arsenite in aquatic systems, Journal of Industrial and Engineering Chemistry 73 (2019) 205–213. https://doi.org/10.1016/j.jiec.2019.01.026

Hu C, Liu H, Chen G, Qu J, Effect of aluminum speciation on arsenic removal during coagulation process, Separation and Purification Technology 86 (2012) 35–40. http://dx.doi.org/10.1016/j.seppur.2011.10.017

Ismahane B, Mohamed B, Mohamed T, François L,Kenza B, Assessment of electrocoagulation based on nitrate removal, for treating and recycling the Saharan groundwater desalination reverse osmosis concentrate for a sustainable management of Albien resource, Journal of Environmental Chemical Engineering 7 (2019) 102951. https://doi.org/10.1016/j.jece.2019.102951

João F.A. Silva, Nuno S. Graça, Ana M. Ribeiro, Alírio E. Rodrigues, Electrocoagulation process for the removal of co-existent fluoride, arsenic and iron from contaminated drinking water, Separation and Purification Technology 197 (2018) 237–243. https://doi.org/10.1016/j.seppur.2017.12.055

Kanika S, Urmila B, Aditya C, Coagulation of humic acid and kaolin at alkaline pH: Complex mechanisms and effect of fluctuating organics and turbidity, Journal of Water Process Engineering 31 (2019) 100875. https://doi.org/10.1016/j.jwpe.2019.100875

Khalid SH, Andy S, Rafid AK, Montserrat OP, David P, Defluoridation of drinking water using a new flow column-electrocoagulation reactor (FCER) - Experimental, statistical, and economic approach, Journal of Environmental Management 197 (2017) 80-88. http://dx.doi.org/10.1016/j.jenvman.2017.03.048

Khalid SH, Andy S, Rafid K , Montserrat OP, David P, Energy efficient electrocoagulation using a new flow column reactor to remove nitrate from drinking water e Experimental, statistical, and economic approach, Journal of Environmental Management 196 (2017) 224-233. http://dx.doi.org/10.1016/j.jenvman.2017.03.017

Kim JH, An B, Lim DH, Park JY, Electricity production and phosphorous recovery as struvite from synthetic wastewater using magnesium-air fuel cell electrocoagulation, Water Research 132 (2018) 200-210. https://doi.org/10.1016/j.mtener.2020.100499

Kim JH, Hubdar A M, Park JY, Treatment of synthetic arsenate wastewater with iron-air fuel cell electrocoagulation to supply drinking water and electricity in remote areas, Water Research 115 (2017) 278-286. http://dx.doi.org/10.1016/j.watres.2017.02.066

Kim JH, Park IS, Park JY, Electricity generation and recovery of iron hydroxides using a single chamber fuel cell with iron anode and air-cathode for electrocoagulation, Applied Energy 160 (2015) 18–27. http://dx.doi.org/10.1016/j.apenergy.2015.09.041

Kong Y, Ma Y, Ding L, Ma J, Zhang H, Chen Z, Shen J, Coagulation behaviors of aluminum salts towards humic acid: detailed analysis of aluminum speciation and transformation, Separation and Purification Technology 259 (2021) 118137. https://doi.org/10.1016/j.seppur.2020.118137

Liu J, Fan J, He T, Xu X, Ai Yulu, Tang H, Gu H, Lu T, Liu Y, Liu G, The mechanism of aquatic photodegradation of organophosphorus sensitized by humic acid-Fe^{3+} complexes, Journal of Hazardous Materials 384 (2020) 121466.

https://doi.org/10.1016/j.jhazmat.2019.121466

Manuel G, Sergio C, Paula O, Mario D, The wet oxidation of aqueous humic acids, Journal of Hazardous Materials 396 (2020) 122402. https://doi.org/10.1016/j.jhazmat.2020.122402

M. Elazzouzi, Kh. Haboubi, M.S. Elyoubi, Electrocoagulation flocculation as a low-cost process for pollutants removal from urban wastewater, chemical engineering research and design 117 (2017) 614-626. http://dx.doi.org/10.1016/j.cherd.2016.11.011

Murat E, Mustafa K, Tugrul S A, Ebubekir Y, The effects of alternating current electrocoagulation on dye removal from aqueous solutions, Chemical Engineering Journal 153 (2009) 16–22. https://doi.org/10.1016/j.cej.2009.05.028

N.P.Tanattı, İ. A. Şengil, A. Özdemir, Optimizing TOC and COD removal for the biodiesel wastewater by electrocoagulation, Applied Water Science (2018) 8:58. https://doi.org/10.1007/s13201-018-0701-2

P. Goel, D. Dobhal, R.C. Sharma, Aluminum–air batteries: A viability review, Journal of Energy Storage 28 (2020) 101287. https://doi.org/10.1016/j.est.2020.101287

Petros K, Vasiliki M, Constantin P, George A, Panagiotis L, Study of some basic operation conditions of an Al-air cell using technical grade commercial aluminum, Journal of Power Sources 450 (2020) 227624. https://doi.org/10.1016/j.jpowsour.2019.227624

Sergi GS, Maria Maesia S.G. E, Jailson V de M, Carlos Alberto Martínez-Huitle, Electrocoagulation and advanced electrocoagulation processes: A general

review about the fundamentals, emerging applications and its association

with other technologies, Journal of Electroanalytical Chemistry 801 (2017) 267–299. http://dx.doi.org/10.1016/j.jelechem.2017.07.047

Son MH, Gong J, Seo S, Yoon H, Chang YS, Photosensitized diastereoisomer-specific degradation of hexabromocyclododecane (HBCD) in the presence of humic acid in aquatic systems, Journal of Hazardous Materials 369 (2019) 171–179. https://doi.org/10.1016/j.jhazmat.2019.02.035.

Song J, Jin X, Wang X C., Jin P, Preferential binding properties of carboxyl and hydroxyl groups with aluminium salts for humic acid removal, Chemosphere 234 (2019) 478-487. https://doi.org/10.1016/j.chemosphere.2019.06.107

Subramanyan V, Jothinathan L, Ganapathy S, Effects of alternating and direct current in electrocoagulation process on the removal of cadmium from water, Journal of Hazardous Materials 192 (2011) 26–34. https://doi.org/10.1016/j.jhazmat.2011.04.081

Surendra SKJ, Ashish PU, Rajesh V, Sivakumar P, Manish KS, Swapnil D, Adsorptionandrecyclabilityaspectsofhumicacidusing nano-ZIF-8adsorbent, Environmental Technology & Innovation 19 (2020) 100927. https://doi.org/10.1016/j.eti.2020.100927

Wang JN, Li AM, Zhou Y, Xu L, Study on the influence of humic acid of different molecular weight on basic ion exchange resin's adsorption capacity, Chinese Chemical Letters 20 (2009) 1478–1482. https://doi.org/10.1016/j.cclet.2009.07.013

Wu S, Zhang Q, Ma J, Sun D, Tang Y, Wang H, Interfacial design of Al electrode for efficient aluminum-air batteries:issues and advances, Materials Today Energy 18 (2020)

100499.https:/doi.org/10.1016/j.mtener.2020.100499

Wu Z, Zhang H, Yang D, Zou J, Qin K, Ban C, Cui J, Hiromi N, Electrochemical behaviour and discharge characteristics of an Al-Zn-In-Sn anode for Al-air batteries in an alkaline electrolyte, Journal of Alloys and Compounds 837 (2020) 155599. https://doi.org/10.1016/j.jallcom.2020.155599

Xie L, Lu Q, Mao X, Wang J, Han L, Hu J, Lu Q, Wang Y, Zeng H, Probing the intermolecular interaction mechanisms between humic acid and different substrates with implications for its adsorption and removal in water treatment, Water Research 176 (2020) 115766. https://doi.org/10.1016/j.watres.2020.115766

Xu H, Jiao R, Xiao F, Wang D, Enhanced removal for humic-acid (HA) and coagulation process using carbon nanotubes (CNTs)/polyalumium chloride (PACl) composites coagulants, Colloids and Surfaces A: Physicochem. Eng. Aspects 490 (2016) 189–199. http://dx.doi.org/10.1016/j.colsurfa.2015.11.047

Yin H, Guo Q, Lei C, Chen W, Huang B, Electrochemical-driven carbocatalysis as highly efficient advanced oxidation processes for simultaneous removal of humic acid and Cr(VI), Chemical Engineering Journal 396 (2020) 125156. https://doi.org/10.1016/j.cej.2020.125156

Zhang J, Ning F, Kang M, Ma C, Qiu Z, Effective removal of humic acid from aqueous solution using adsorbents prepared from the modified waste bamboo powder, Microchemical Journal 153 (2020) 104272. https://doi.org/10.1016/j.microc.2019.104272

Zhao S, Sun Q, Gu Y, Yang W, Chen Y, Lin J, Dong M, Cheng H, Hu H, Guo Z, Enteromorpha prolifera polysaccharide based coagulant aid for humic acids removal and ultrafiltration membrane fouling control, International Journal of Biological Macromolecules 152 (2020) 576–583. https://doi.org/10.1016/j.ijbiomac.2020.02.273

Zhou XF, Liang JP, Zhao ZL, Yuan H, Qiao JJ, Xu QN, Wang HL, Wang WC, Yang DZ, Ultra-high synergetic intensity for humic acid removal by coupling bubble discharge with activated carbon, Journal of Hazardous Materials 403 (2021) 123626. https://doi.org/10.1016/j.jhazmat.2020.123626

Figures

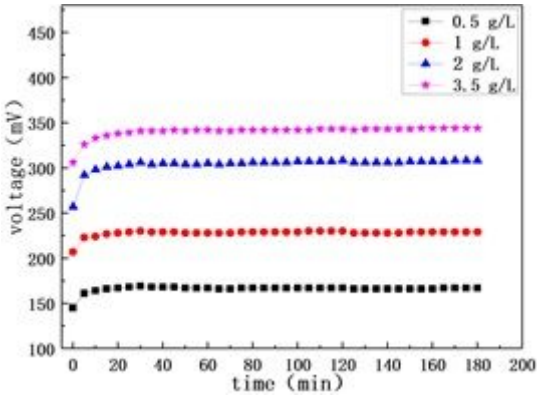

Figure 1

Voltage according to operation time for different NaCl concentrations

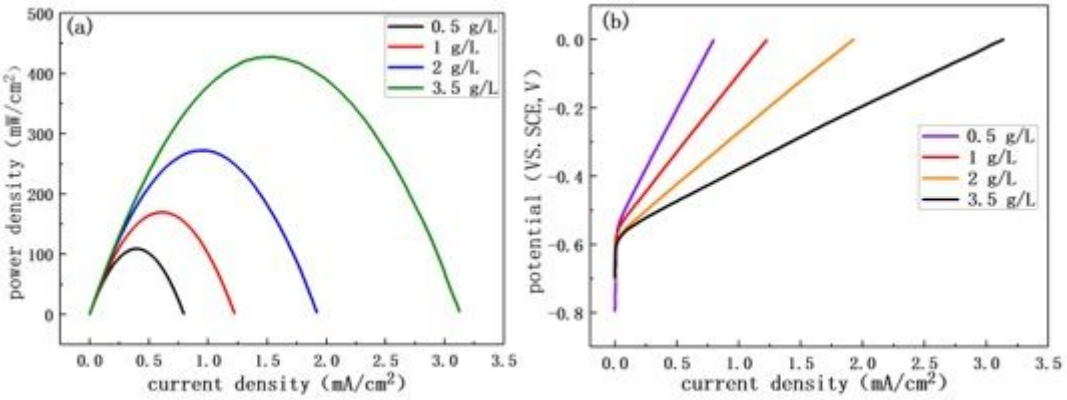

Figure 2

(a) Power density and (b) anode potential according to current density for different NaCl concentrations

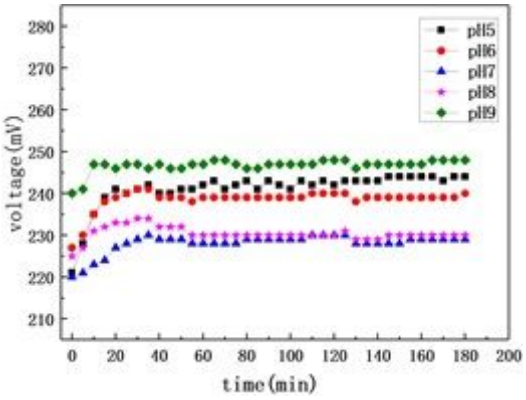

Figure 3

Voltage according to operation time for different initial pH

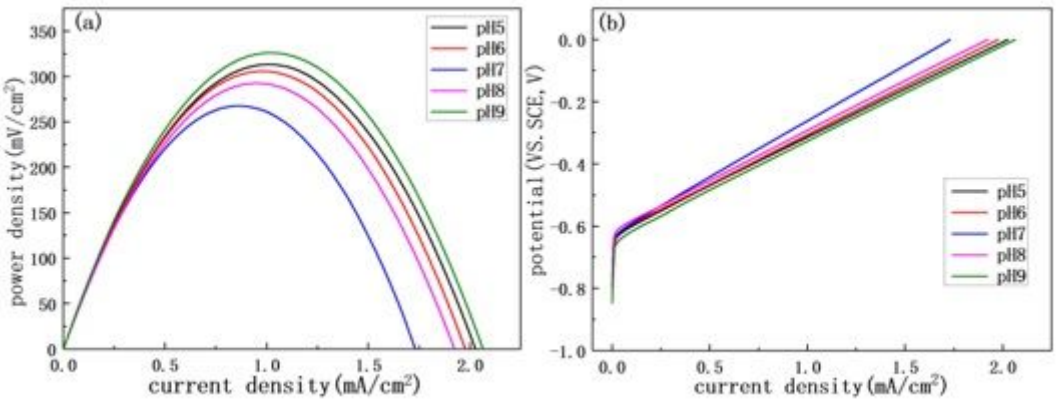

Figure 4

(a) Power density and (b) anode potential at different initial pH

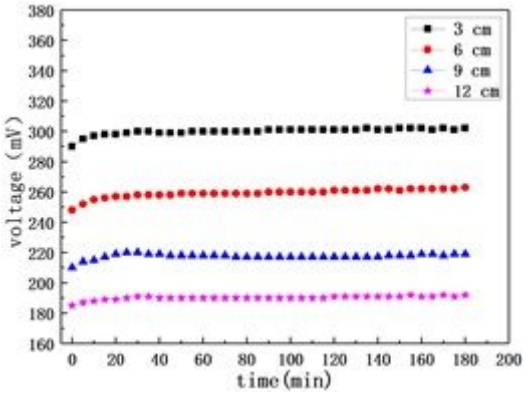

Figure 5

Voltage according to time for different electrode distance

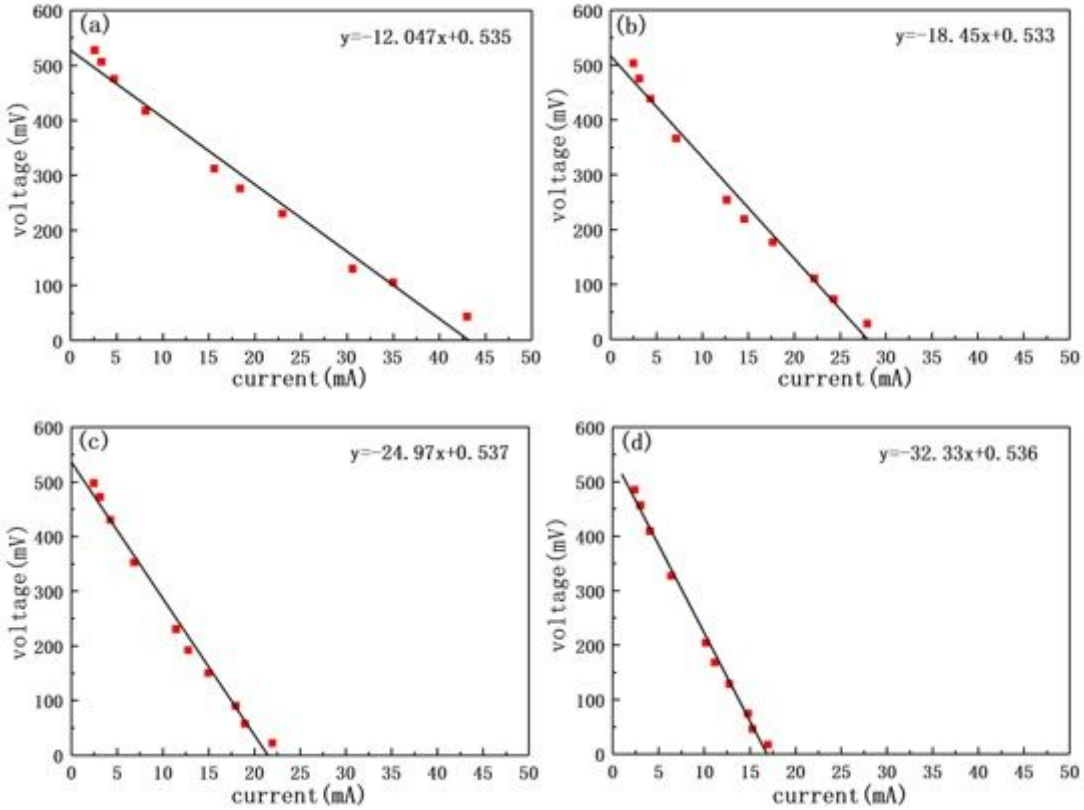

Figure 6

Volt–ampere characteristics for electrode distances of (a) 3, (b) 6, (c) 9, and (d) 12 cm.

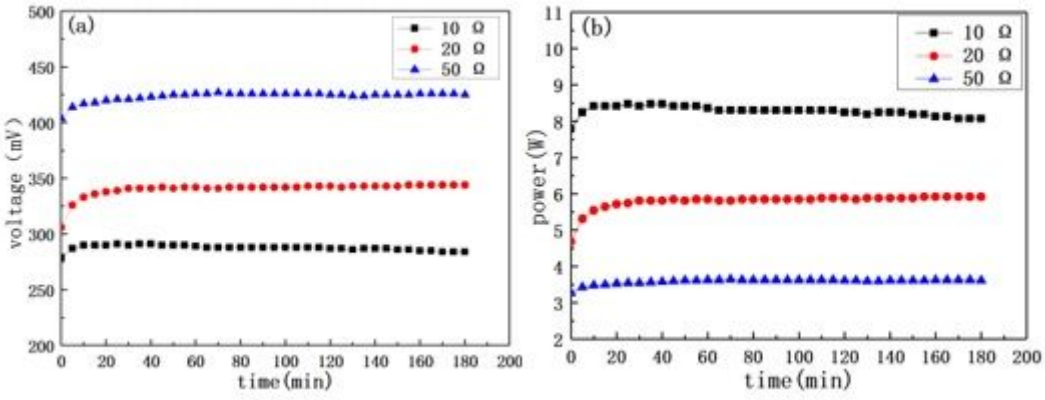

Figure 7

(a) Voltage and (b) output power according to time for different external resistance

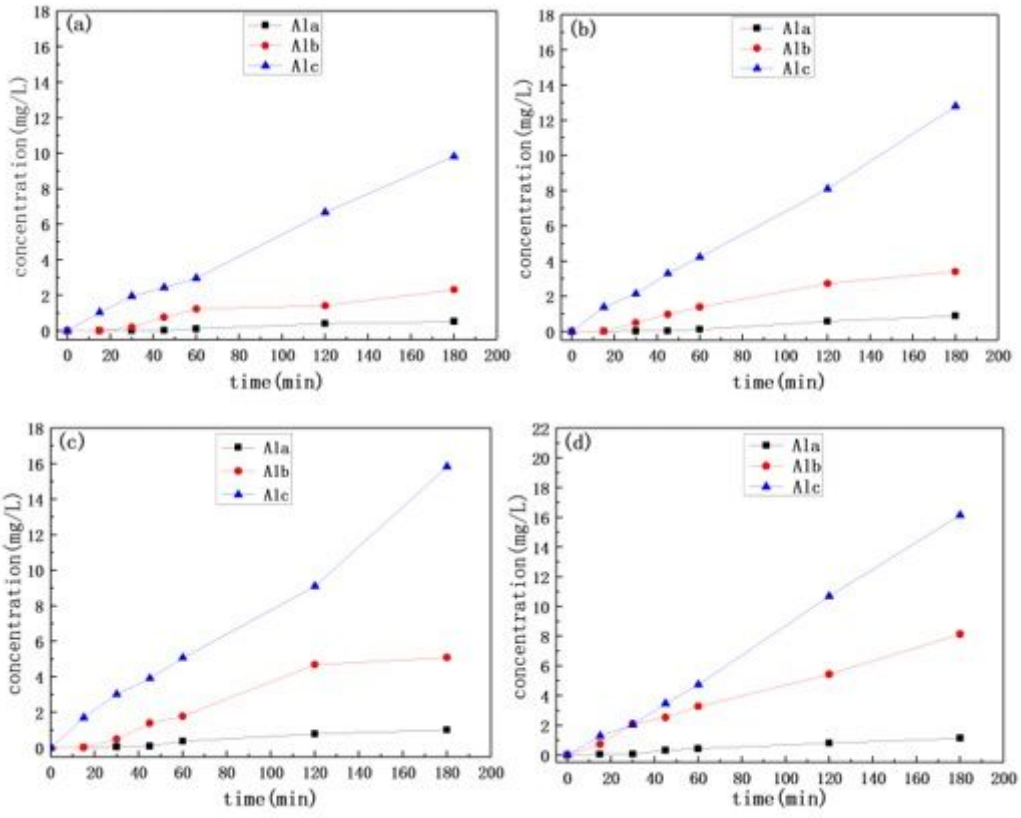

Figure 8

Aluminum speciation distribution according to time for NaCl solution concentrations of (a) 0.5, (b) 1, (c) 2, and (d) 3.5 g/L

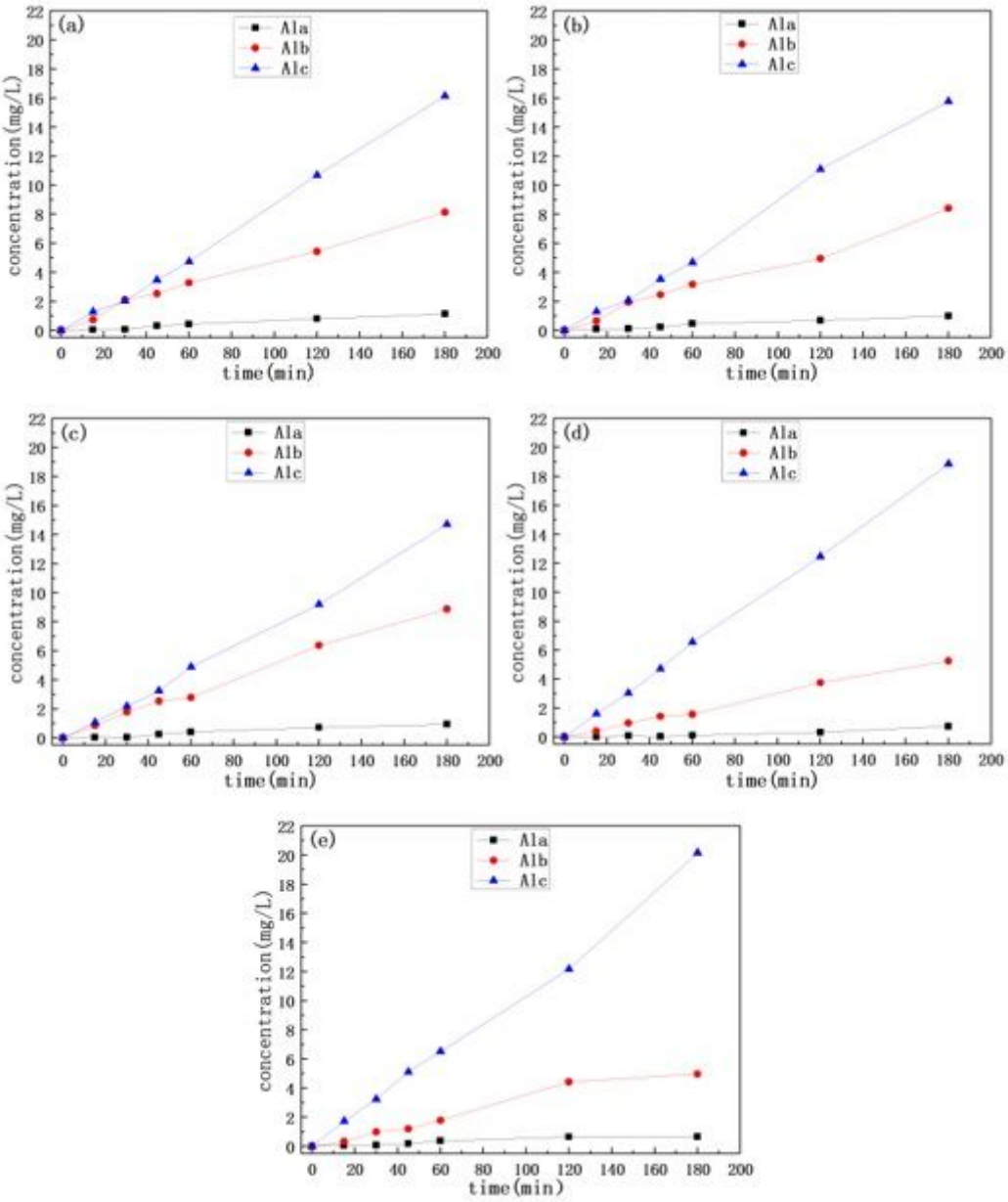

Figure 9

Aluminum speciation distribution according to time for different initial pH of (a) 5, (b) 6, (c) 7, (d) 8, and (e) 9

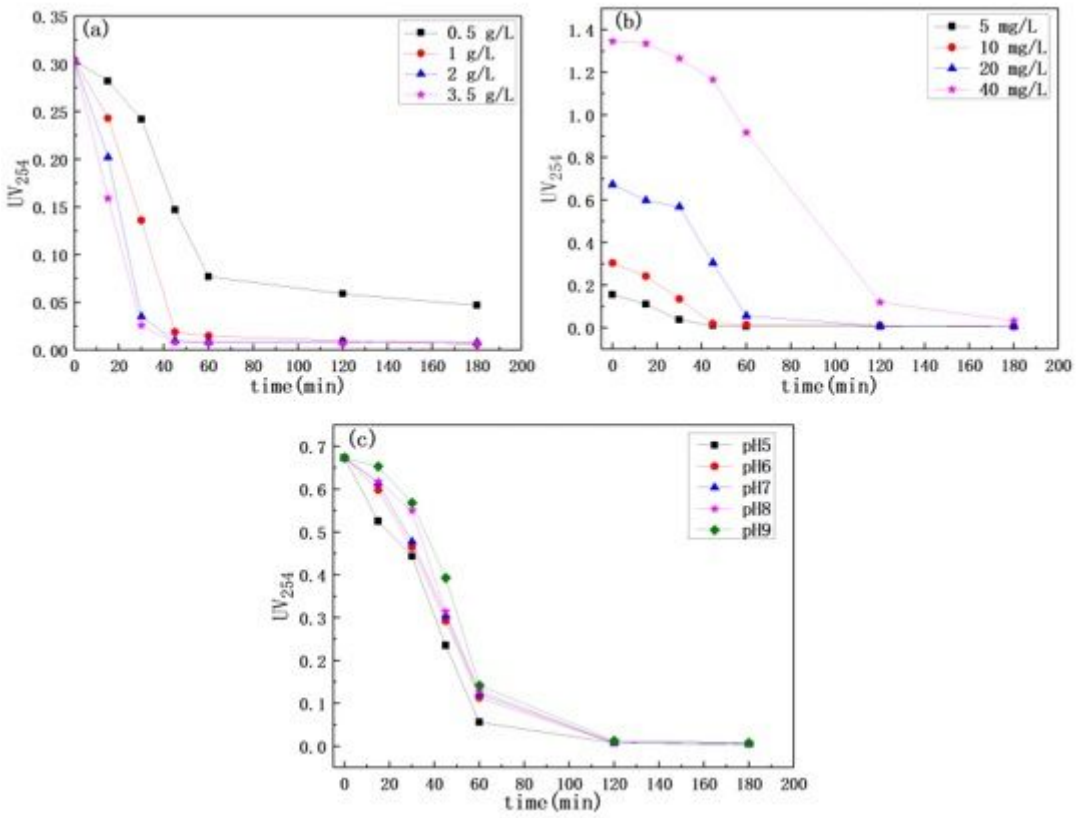

Figure 10

UV254 according to time under different parameters conditions: (a) NaCl concentration, (b) humic acid concentration, and (c) initial pH

Supplementary Files

This is a list of supplementary files associated with this preprint. Click to download.

- GraphicalAbstract.docx